

1 **Measurement report: Distinct Emissions and Volatility Distribution of Intermediate**  
2 **Volatility Organic Compounds from on-road Chinese Gasoline Vehicle: Implication of**  
3 **High Secondary Organic Aerosol Formation Potential**

4 Rongzhi Tang<sup>1,2,3,#</sup>, Quanyang Lu<sup>4,#</sup>, Song Guo<sup>1,3,\*</sup>, Hui Wang<sup>1</sup>, Kai Song<sup>1</sup>, Ying Yu<sup>1</sup>, Rui Tan<sup>1</sup>,  
5 Kefan Liu<sup>1</sup>, Ruizhe Shen<sup>1</sup>, Shiyi Chen<sup>1</sup>, Limin Zeng<sup>1</sup>, Spiro D. Jorga<sup>4</sup>, Zhou Zhang<sup>5</sup>, Wenbin  
6 Zhang<sup>5</sup>, Shijin Shuai<sup>5</sup>, Allen L. Robinson<sup>4,\*</sup>

7 *1 State Key Joint Laboratory of Environmental Simulation and Pollution Control, International*  
8 *Joint Laboratory for Regional Pollution Control, Ministry of Education (IJRC), College of*  
9 *Environmental Sciences and Engineering, Peking University, Beijing 100871, China P. R.*

10 *2 School of Environmental and Material Engineering, Yantai University, Yantai, 264003, PR*  
11 *China*

12 *3 Collaborative Innovation Center of Atmospheric Environment and Equipment Technology,*  
13 *Nanjing University of Information Science & Technology, Nanjing 210044, China P. R.*

14 *4 Department of Mechanical Engineering and Center for Atmospheric Particle Studies, Carnegie*  
15 *Mellon University, 5000 Forbes Avenue, Pittsburgh, Pennsylvania 15213, United States*

16 *5 State Key Laboratory of Automotive Safety and Energy, School of Vehicle and Mobility, Tsinghua*  
17 *University, Beijing, 100084, PR China*

18 Correspondence to: S. Guo [songguo@pku.edu.cn](mailto:songguo@pku.edu.cn), A. Robinson: [alr@andrew.cmu.edu](mailto:alr@andrew.cmu.edu)

19 <sup>#</sup>These authors contribute equally to this work

20

21 **Abstract**

22 In the present work, we performed chassis dynamometer experiments to  
23 investigate the emissions and secondary organic aerosol (SOA) formation potential of  
24 intermediate volatility organic compounds (IVOCs) from an on-road Chinese gasoline  
25 vehicle. High IVOCs emission factors (EFs) and distinct volatility distribution were  
26 recognized. The IVOCs EFs for the China V vehicle ranged from 12.1 to 226.3  
27 mg kg-fuel<sup>-1</sup>, with a median value of 83.7 mg kg-fuel<sup>-1</sup>, which was higher than that  
28 from US vehicles. Besides, large discrepancy in volatility distribution and chemical  
29 composition of IVOCs from Chinese gasoline vehicle exhaust was discovered, with  
30 larger contributions of *B*<sub>14</sub>-*B*<sub>16</sub> compounds (retention time bins corresponding to  
31 *C*<sub>14</sub>-*C*<sub>16</sub> *n*-alkanes) and higher percentage of *n*-alkanes. Further we investigated the  
32 possible reasons that influence the IVOCs EFs and volatility distribution and found  
33 that fuel type, starting mode, operating cycles and acceleration rates did have an  
34 impact on the IVOCs EF. When using E10 (ethanol volume ratio of 10%, v/v) as fuel,  
35 the IVOCs EF of the tested vehicle was lower than that using commercial China  
36 standard V fuel. The average IVOC-to-THC ratios for gasoline-fueled and E10-fueled  
37 gasoline vehicle were 0.07 ± 0.01 and 0.11 ± 0.02, respectively. Cold-start operation  
38 had higher IVOCs EF than hot-start operation. Chinese Light vehicles Test Cycle  
39 (CLTC) produced 70% higher IVOCs than those from the World-wide harmonized  
40 Light-duty Test Cycle (WLTC). We found that the tested vehicle emitted more IVOCs  
41 at lower acceleration rates, which leads to high EFs under CLTC. The only factor that  
42 may influence the volatility distribution and compound composition is the  
43 engine-aftertreatment system, which has compound and volatility selectivity in  
44 exhaust purification. These distinct characteristics in EFs and volatility may result in  
45 higher SOA formation potential in China. Using published yield data and surrogate  
46 equivalent method, we estimated SOA formation under different OA loading and NO<sub>x</sub>  
47 conditions. Results showed that under low and high NO<sub>x</sub> conditions at different OA  
48 loadings, IVOCs contributed more than 80% of the predicted SOA. Furthermore, we  
49 built up a parameterization method to simply estimate the vehicular SOA based on our  
50 bottom-up measurement of VOCs and IVOCs, which would provide another

51 dimension of information when considering the vehicular contribution to the ambient  
52 OA. Our results indicate that vehicular IVOCs contribute significantly to SOA,  
53 implying that the importance of reducing IVOCs when making air pollution  
54 controlling policies in urban area of China.  
55

## 56 **1 Introduction**

57 Atmospheric fine particulate matter has great impacts on human health, regional  
58 air pollution, and global climate (Hallquist et al., 2009;Guo et al., 2014b). Organic  
59 aerosols are a major component of fine particulate matter. Secondary organic aerosol  
60 (SOA), formed from multiple generations of oxidation of thousands of organic gases  
61 and vapors, contribute 30% or more of organic aerosols in different areas of the world  
62 (Zhang et al., 2007). It has great impact on various other atmospheric processes, e.g.  
63 new particle formation and growth, and black carbon aging (Guo et al., 2020;Peng et  
64 al., 2016;Guo et al., 2016). Due to its complexity in sources and photochemical  
65 processes, SOA formation remains uncertain (Tang et al., 2019;Wang et al., 2020;Guo  
66 et al., 2014a).

67 A large discrepancy remains between modeled and measured SOA. One possible  
68 reason is missing SOA precursors. Apart from traditional SOA precursors, i.e. volatile  
69 organic compounds (VOCs), Robinson et al. (2007) proposed intermediate volatility  
70 organic compounds (IVOCs) as important contributors to SOA formation. IVOCs are  
71 less volatile than VOCs with effective saturation concentrations in the range of  $10^3$  to  
72  $10^6 \mu\text{g}/\text{m}^3$  (Donahue et al., 2006), roughly corresponds to the volatility range of  
73  $\text{C}_{12}$ - $\text{C}_{22}$  *n*-alkanes. IVOCs exist mainly in the gas phase under typical atmospheric  
74 conditions. Previous studies demonstrate that IVOCs may be important SOA  
75 precursors both in ambient air and in typical source emissions i.e. gasoline vehicles,  
76 diesel vehicles and ship emissions (Huang et al., 2018;Zhao et al., 2016, 2015;Zhao et  
77 al., 2014;Yu et al., 2020). Recent model studies have shown that adding IVOC  
78 emissions into different models will greatly improve the SOA simulation results. For  
79 example, Giani et al. (2019) found a considerable OA enhancement in Po Valley  
80 (Northern Italy) when applying new S/IVOCs emission estimates and the new  
81 volatility distributions into CAMx, in which the improvement in SOA mainly due to  
82 the revised IVOC emissions. Huang et al. (2020) found a similar enhancement in SOA  
83 simulation for Yangtze River Delta (Southeast China) region when adding IVOC  
84 emissions into CAMx. They also show the importance of volatility distribution and  
85 emission parameterization for the model simulation. Therefore, understanding and

86 characterizing IVOC emissions, as well as their volatility distributions, is crucial for  
87 improving numerical models that aim to predict OA.

88 China is in a high-growth stage with rapidly increasing number of on-road  
89 vehicles (~26 fold in 25 years). This growth has created a substantial burden on air  
90 quality and human health (Hallquist et al., 2016;Hu et al., 2015). Anthropogenic  
91 emissions have become the major contributors to both primary and secondary  
92 particles in megacities of China (Tang et al., 2018;Guo et al., 2012b). During the past  
93 few years, many researchers have studied the gases and particulate matter emissions  
94 from Chinese vehicles (Cao et al., 2016;Huang et al., 2015). However, none of these  
95 studies have reported data on IVOCs emissions from Chinese gasoline vehicles.  
96 Although Zhao et al. (2016) characterized IVOC emission in gasoline vehicles in the  
97 United States, the results may not be applicable to China given differences in vehicle  
98 technologies, operating conditions, and fuel quality. Therefore, understanding and  
99 characterizing the IVOC emissions, as well as their volatility distributions from  
100 Chinese vehicle, is of vital importance to understand the contribution of IVOCs to  
101 SOA formation in China.

102 In this study, IVOCs emissions were measured from a China V gasoline vehicle  
103 equipped with a direct inject (GDI) engine during chassis dynamometer testing. The  
104 test matrix considered the influence of fuel type and operating conditions on the total  
105 IVOC emission factors, including a newly designed cycle designed to simulate  
106 Chinese driving conditions. All of the measurements were performed with the same  
107 gasoline vehicle in order to consistently evaluate the effects of these different factors  
108 on IVOC emissions. The emission factors (EFs), volatility and chemical speciation of  
109 IVOC emissions from different conditions were investigated, and the SOA formation  
110 potential were estimated.

111

## 112 **2 Materials and Methods**

### 113 **2.1 Testing Vehicle, Fuels and Test Cycles**

114 In this study, all measurements were performed on a vehicle chassis  
115 dynamometer (Peng et al., 2017) using an in-use light-duty gasoline direct inject (GDI)

116 engine vehicle meeting the China V standard (similar to Euro 5). Tests were  
117 conducted with two fuels: commercial China Standard V gasoline and E10 fuel (10%  
118 ethanol by volume). The test cycles included the World-wide harmonized Light duty  
119 Test Cycle (WLTC), and the Chinese Light vehicles Test Cycle (CLTC). Furthermore,  
120 typical different acceleration rates were also tested. Detailed description and speed  
121 profiles of WLTC and CLTC are in Figure S1 in the supplementary information. The  
122 CLTC was specifically designed to simulate the driving patterns in Chinese cities  
123 while WLTC referred to the Euro VI standard and adopted as China VI testing  
124 protocol. Prior to tests, the tested vehicle was preconditioned with an overnight soak,  
125 without evaporative canister purge. Different acceleration rates were selected based  
126 on their frequency in both CLTC and WLTC, i.e. 1.2, 3.6 6.0 km/h/s, written as  
127 ACR1.2, ACR3.6 and ACR6.0), to investigate the effects of acceleration rates on  
128 IVOC emissions. All three acceleration “cycles” last for 600 s with a maximum  
129 velocity of 70 km/h. The acceleration driving cycles were set according to the criteria  
130 of identical cycle period and maximum velocity, and hence the mean velocity for each  
131 acceleration cycle is the same (Figure S2). We also measured IVOC emission factors  
132 (EFs) when the test vehicle was idling.

133

## 134 **2.2 Sampling and Chemical Analysis**

135 Tailpipe emissions were introduced to a constant volume sampler (CVS) that  
136 diluted the exhaust by a factor of 20 to 40. For WLTC and CLTC tests, IVOCs  
137 emissions were collected by sampling the diluted exhaust through a quartz filter  
138 followed by two tandem Tenax TA filled glass tubes (Gerstel, 6 mm OD, 4.5 mm ID  
139 glass tube filled with ~180 mg Tenax TA). Sampling tubes and transfer lines from the  
140 CVS were kept at a constant temperature ( $27 \pm 2$  °C). The flow rate for quartz filter  
141 was 10.0 L/min, and the flow rate for Tenax tube was set as 0.5 L/min. Dynamic  
142 blanks were also collected when the CVS was operated with only dilution air (no  
143 exhaust) to estimate the contribution of background organic vapors. Prior to sampling,  
144 the quartz filters were preheated to 550 °C in air for 6 h in clean aluminum foil using  
145 a muffle furnace to remove contaminations. Tenax tubes were preconditioned by using

146 Tube Conditioner (BCT700, BCT Technology LTD), at 300 °C for 3 h in pure  
147 nitrogen with a constant flow rate of 100 mL/min. All samples were sealed after  
148 sampling and stored in freezer at -20°C.

149 Quartz filters and Tenax tubes were analyzed using a gas chromatography/mass  
150 spectrometry (Agilent 6890GC/5975MS) equipped with a capillary column (Agilent  
151 HP-5MS, 30 m × 0.25 mm) coupled to a thermal desorption system (Gerstel, Baltimore,  
152 MD). The detailed method was described by Zhao et al.(2014). Prior to analysis, 5 µl  
153 of the internal standards (*d*10-acenaphthene, *d*12-chrysene, *d*4-1,4-dichlorobenzene,  
154 *d*8-naphthalene, *d*12-perylene, *d*10-phenanthrene and 7 deuterated *n*-alkanes) were  
155 injected into each adsorbent tube to track the IVOCs recovery.

156 For each test, particulate matter samples were also collected using independent  
157 Teflon and quartz filters. The Teflon filters were weighted using a microbalance  
158 (Toledo AX105DR, USA) after equilibration for 24 h in an environmental controlled  
159 room (temperature 20 ± 1°C, relative humidity 40 ± 3%) (Guo et al., 2010). A punch  
160 (1.45 cm<sup>2</sup>) from each quartz filter was analyzed for organic carbon (OC) and  
161 elemental carbon (EC) via thermal-optical method using Sunset Laboratory-based  
162 instrument (NIOSH protocol, TOT) (Guo et al., 2012a). VOCs were sampled in  
163 SUUMA® polished stainless steel canisters and analyzed using GC-MS with a flame  
164 ionization detector. Total hydrocarbon (THC), nitrogen oxide, CO and CO<sub>2</sub> emissions  
165 under operation scenarios were measured using a Horiba OBS 2200 portable emission  
166 system.

167

### 168 **2.3 Quantification of IVOCs**

169 Twenty IVOCs compounds were quantified using authentic standards (Table S1).  
170 However, the majority of the IVOCs mass appears as a broad hump of co-eluting  
171 hydrocarbons and oxygenated organics. These compounds could not be resolved at  
172 the molecular level and were therefore classified as an unresolved complex mixture  
173 (UCM), which were grouped based on their volatilities.

174 The total mass of IVOCs was determined following the method of Zhao et al.  
175 (2014) (SI). In short, the TIC of each sample was divided into 11 retention time bins

176 corresponding to C<sub>12</sub>-C<sub>22</sub> *n*-alkanes. The total mass in each bin was estimated using  
177 the instrument response to the *n*-alkane in that bin. UCM was determined as the  
178 difference between total IVOCs and speciated IVOCs in each bin. UCM was then  
179 further classified into unspciated branched alkanes (*b*-alkanes) and unspciated  
180 cyclic compounds following the approach of Zhao et al. (2016) (SI). The uncertainty  
181 of the IVOCs could be ascribed to both sampling and analysis. The sampling  
182 uncertainty was assumed as 10% (Huang et al., 2019). The uncertainty of using  
183 *n*-alkanes as surrogate standards for the total IVOC mass was estimated to be less than  
184 6.0% for alkanes and 30.6% for PAHs based on the analysis of a suite of standard  
185 compounds (SI). Therefore, combined the above uncertainty, we consider a maximum  
186 IVOCs mass uncertainty of 32.2% (SI).

187 Fuel-based IVOC emission factors (EF, mg/kg-fuel) were calculated using the  
188 carbon-mass-balance method as following:

$$189 \quad EF_{IVOCs} = \frac{[\Delta IVOC]}{[\Delta CO_2]} f_c$$

190 where [Δ IVOC] represents the background-corrected mass concentration of  
191 IVOCs, [ΔCO<sub>2</sub>] is the background-corrected CO<sub>2</sub> concentration in the CVS expressed  
192 in units of carbon mass and *f<sub>c</sub>* is the measured mass fraction of carbon in the gasoline  
193 (0.82).

194

## 195 **3 Results and Discussion**

### 196 **3.1 Influence of Fuel, Starting Mode, and Operating Cycles on IVOC Emission**

#### 197 **Factors**

198 Figure 1 depicts IVOC EFs of the tested China V gasoline vehicle and compares  
199 them with previous studies. The IVOC EFs ranged from 12.1 to 226.3 mg kg-fuel<sup>-1</sup>,  
200 with a median value of 83.7 mg kg-fuel<sup>-1</sup>. The median IVOC value was ~3 times  
201 higher than that of the US LEV-2 gasoline vehicles (21.9 mg kg-fuel<sup>-1</sup>), and one order  
202 of magnitude lower than diesel-fueled non-road construction machinery and a  
203 diesel-fueled large cargo vessel (971.1 and 800 mg kg-fuel<sup>-1</sup>, respectively) (Qi et al.,  
204 2019;Huang et al., 2018).

205 Figure 1 summarizes the influences of fuel type, starting mode, operating cycles  
206 and acceleration rates on the total IVOC EFs. Various operating conditions may cause  
207 different IVOCs emission and fuel consumption. In order to get a relative reliable  
208 comparison, what we show here is all described in IVOCs EFs which consider both  
209 IVOCs mass and the fuel consumption. Among all of the factors, acceleration rate has  
210 the largest influence on the IVOC EFs. The fuel consumption at high acceleration rate  
211 (6.0 km/h/s) would be higher than that at low acceleration rate (idling). Although not  
212 emitted in IVOCs, the high consumption of the fuel would exist as other types of  
213 carbon e.g. VOCs and CO<sub>2</sub> which may also have great effects on the atmosphere.  
214 Therefore, the usage of IVOCs EFs can moderately balance the effects of the IVOCs  
215 emission and fuel consumption and get a comprehensive comparison among different  
216 acceleration rates. As the acceleration rate increases, the IVOC EF decreases, with the  
217 median IVOC EF of ACR6.0 being one order of magnitude lower than that at idling.  
218 Qi et al. (2019) and Zhao et al. (2016) report similar results for non-road construction  
219 machinery and on-road diesel vehicles, where idling conditions emitted significantly  
220 higher IVOCs than those under higher-speed cycles. They proposed that the higher  
221 IVOC EFs at idling were the result of less efficient fuel combustion. An additional  
222 factor in these tests may be the efficiency of the catalytic converter varying with  
223 operating conditions (i.e. lower efficiency at idle operations).

224 When using commercial China Standard V gasoline, the median IVOC EF was  
225 1.4 times greater than that using Ethanol gasoline, i.e. E10 (10% ethanol, v/v), with  
226 median values of 91.5, and 67.6 mg kg-fuel<sup>-1</sup>, respectively. The median THC EFs for  
227 gasoline and E10 were 485 and 589 mg kg-fuel<sup>-1</sup>, respectively, showing no significant  
228 difference.

229 As expected, The IVOC EFs for cold-start tests was higher (83.7 mg kg-fuel<sup>-1</sup>)  
230 than those for hot-start tests (58.7 mg kg-fuel<sup>-1</sup>). This reflects the reduced efficiency  
231 of the catalytic converter during cold-start operation. The cold-start to hot-start IVOC  
232 emission ratio is about 1.4, which is similar to the previous study (Zhao et al., 2016).  
233 The median THC EFs for cold-start and hot-start tests are 556.2 and 507.8  
234 mg kg-fuel<sup>-1</sup>, respectively. Previous studies also show that cold starts have higher

235 THC EFs than hot start operation, but cold-to-hot ratios can span a wide range due to  
236 differences in operating conditions and model years (Jaworski et al., 2018; Drozd et al.,  
237 2016). The ratio is generally larger for more modern, heavily controlled vehicles  
238 (Saliba et al., 2017; May et al., 2014).

239 The median IVOC EF for CLTC was about 1.7 times of that for WLTC (103.5  
240 versus 60.9 mg kg-fuel<sup>-1</sup>). Similar results were also found for THC emission, with  
241 median THC EFs for CLTC and WLTC cycle as 617.3 and 420.3 mg kg-fuel<sup>-1</sup>,  
242 respectively. Previous studies also show test cycles influence THC EFs. For example,  
243 Suarez-Bertoa et al. (2015) and Marotta et al. (2015) found that the NEDC cycle has  
244 higher THC EFs than WLTP or WLTC cycle. One possible explanation for the  
245 differences between the CLTC and WLTC IVOC EFs is the differences in acceleration  
246 rates. A histogram of acceleration rates of the two cycles (Figure S3) shows that  
247 CLTC has frequent low acceleration process compared to WLTC. 76.9% of the CLTC  
248 has acceleration rates ranging from -1.5 to 1.5 km/h/s versus 69.6% for the WLTC.  
249 The CLTC has no acceleration rate higher than 4 km/h/s, suggesting that the gasoline  
250 vehicles frequently drive in congested conditions in China.

251 The results from the acceleration rate cycles suggest that the frequent low  
252 acceleration rate in CLTC is responsible for the differences of the IVOC EF between  
253 CLTC and WLTC. The effect of acceleration on IVOC EFs is probably especially  
254 important in urban areas in China, which frequently have substantial traffic  
255 congestion. These results underscore the importance of developing cycles that  
256 simulate real-world Chinese driving condition e.g. CLTC, instead of using WLTC or  
257 other cycles to get relevant emissions data.

258

### 259 **3.2 Chemical Speciation of Chinese Vehicle IVOCs and the Relationships** 260 **between Total IVOCs, POA and THC**

261 Figure 2 and S4 compare the chemical composition of IVOC emissions from the  
262 tested China V vehicle under different operating conditions. In general, IVOC  
263 chemical composition was similar across all the tests. Unspeciated IVOCs (UCM)  
264 dominates the total IVOCs mass ( $85.6 \pm 4.9\%$ ), including  $65.2 \pm 5.2\%$  for unspeciated

265 cyclic compounds and  $20.4 \pm 0.7\%$  for unspciated *b*-alkanes. *n*-alkanes and spciated  
266 aromatics contribute  $10.9 \pm 4.7\%$  and  $3.5 \pm 1.7\%$  of the total IVOC mass, respectively.  
267 These results are similar to previous studies. For example, Zhao et al. (2016) found  
268 the consistent composition of IVOC emissions across a wide set of vehicles.

269 Since the majority of the IVOC mass appears as UCM, the average mass spectra  
270 provide additional insight into its composition. A similar distribution of mass  
271 fragments was observed across all tests. Figure 2(b) shows the average IVOC mass  
272 spectrum collected during an E10 CLTC test. Mass fragments associated with  
273 aliphatic hydrocarbons ( $m/z$  43, 57, 71, 85) are the most abundant followed by those  
274 associated with aromatics ( $m/z$  91, 105 and 119 for alkylbenzenes (Pretsch et al.,  
275 2013), and  $m/z$  115, 165, 189 for poly aromatic species) (Dall'Osto et al.,  
276 2009;Spencer et al., 2006).

277 Figures 2(c) and (d) exhibit the contribution of selected mass fragments in low  
278 and high volatility ranges, i.e.  $B_{12}$ - $B_{16}$  and  $B_{17}$ - $B_{22}$ . Aliphatic fragments are higher than  
279 aromatics fragments in both  $B_{12}$ - $B_{16}$  and  $B_{17}$ - $B_{22}$  bins. Compared to the higher  
280 volatility ( $B_{12}$ - $B_{16}$ ) bins, the ratio of selected aromatic to aliphatic fragments is lower  
281 in the lower volatility ( $B_{17}$ - $B_{22}$ ) bins (0.8 versus 1.7) which suggests different  
282 weighting of compounds in different volatility range. Therefore, unspciated IVOC  
283 UCM in  $B_{12}$ - $B_{16}$  are predominantly aromatics while  $B_{17}$ - $B_{22}$  are more abundant in  
284 cyclic alkanes.

285 Figure 3 and S5 shows the volatility distribution of IVOC emissions over the 11  
286 retention-time bins ( $B_{12}$ - $B_{22}$ ). IVOC emissions are more heavily weighted towards the  
287 more volatile end of the distribution, with more than 50% of the emissions in  $B_{12}$ - $B_{14}$   
288 bins. After  $B_{14}$ , the IVOC emission decreases significantly.

289 Although the IVOC EFs varied by an order of magnitude across the set of tests  
290 (Figure 1), the volatility distributions of the emissions were largely the same. When  
291 the vehicle is fueled by gasoline, the median IVOC fractions in the  $B_{12}$ - $B_{14}$  bins are  
292 slightly higher than when fueled by E10 (Figure S5a). Cold-start has a higher median  
293 percentage of IVOC in  $B_{12}$ - $B_{14}$  bins compared to hot-start (Figure S5b). No distinct  
294 differences in volatility differences between the CLTC and WLTC (Figure S5c).

295 Compared with idling condition, acceleration cycles have higher median percentage  
296 of IVOC in lower volatility bins ( $B_{17}-B_{22}$ ) (Figure S5d), similar to previous studies (Qi  
297 et al., 2019; Cross et al., 2015). The modest variations of volatility distributions of the  
298 IVOCs emissions may be due to differences in combustion efficiency and/or catalytic  
299 converter efficiency as a function of volatility.

300 Considering the similarity of volatility distribution for different conditions and  
301 the importance of the volatility distribution in model input for SOA simulation, figure  
302 S6 and Table S3 present the volatility distribution of SVOC and IVOC emissions from  
303 the tested China V gasoline vehicle, using effective saturation concentration ( $C^*$ ) as  
304 classification: IVOCs ( $C^*=300-3 \times 10^6 \mu\text{g}\cdot\text{m}^{-3}$ ), SVOCs ( $C^*=0.3-300 \mu\text{g}\cdot\text{m}^{-3}$ ).  
305 IVOCs are the dominant part of the low volatility organics (IVOCs+SVOCs), with a  
306 median contribution of ~95%.

307 Previous studies have used different scaling approaches to estimate IVOC  
308 emissions using other primary emission data, e.g. POA, NMHC (Murphy et al.,  
309 2017; Woody et al., 2016; Koo et al., 2014). However, these ratios depend on fuel,  
310 engine technology and operating conditions (Lu et al., 2018). Therefore, it is important  
311 to quantify the relationships between IVOCs and other pollutants using data collected  
312 from Chinese vehicles. Our results show that the IVOC-to-THC ratio does depend on  
313 fuel composition. The average IVOC-to-THC ratios for gasoline-fueled and  
314 E10-fueled gasoline vehicle are  $0.07 \pm 0.01$  ( $R^2 = 0.87$ ) and  $0.11 \pm 0.02$  ( $R^2 = 0.78$ ),  
315 respectively (Figure S7). The IVOC-to-THC ratios in this study are higher than US  
316 vehicles (IVOC-to-NMHC of 0.04) (Zhao et al., 2016) but much lower than diesel  
317 fueled vehicles (IVOC-to-THC of 0.67) (Huang et al., 2018). The IVOC-to-POA ratio  
318 was  $5.12 \pm 1.30$  across all tests, but with only modest correlation ( $R^2$  of 0.66 for  
319 gasoline-fueled vehicle and 0.43 for E10-fueled vehicle). This ratio is similar to US  
320 data for gasoline vehicles. The correlation of IVOC to THC or POA in our dataset is  
321 lower than that of the on-road gasoline and diesel vehicles measured in US. This may  
322 be caused to the US data are from a large fleet of vehicles while our data is from a  
323 single vehicle operated over a range of conditions

324

### 3.3 High Emission Factors and Distinct Volatility Distributions of IVOCs from Chinese Gasoline Vehicles

Figure 4 presents PM, NO<sub>x</sub>, THC and IVOC EFs of the tested gasoline vehicle (China V) and compares them to US vehicles tested by Zhao et al. (Zhao et al., 2016;May et al., 2014) For this comparison, we combined all of the CLTC and WLTC data together. The US vehicles are grouped by model year where pre-LEV refers to vehicles manufactured prior to 1994, LEV-1 represents vehicles manufactured between 1994-2003, and LEV-2 indicates vehicles manufactured between 2004-2012.

The emissions of NO<sub>x</sub> and THC from tested vehicle are comparable with those from the newer (LEV-2) US vehicles tested by May et al. (Zhao et al., 2016;May et al., 2014). However, PM EF (44.8 mg kg-fuel<sup>-1</sup>) of the tested vehicle is higher than the LEV-2 vehicles tested (17.0 mg kg-fuel<sup>-1</sup>). It is comparable to a pre-LEV vehicle (61.0 mg kg-fuel<sup>-1</sup>). In addition, we compared our results with that from European vehicles, and found that the NO<sub>x</sub> and THC EFs for the tested vehicle were lower than Euro 5 gasoline vehicle, while the PM EF was higher (Fontaras et al., 2014). This suggests that compared with US and European vehicles, the stringent emission implemented by Chinese government have been effective at controlling NO<sub>x</sub> and THC, but might be inefficient to PM emissions. For past 30 years, Chinese government has adopted a series of emission control policies and measures for light-duty vehicles, including implementation of emission standards for new vehicles promotion of sustainable transportation and alternative fuel vehicles, and traffic management programs (Wu et al., 2017;Zhang et al., 2014). Wu et al. (2017) summarizes the implementation of the vehicle control policies in China, which shows the control for the vehicular pollutants is becoming stricter step by step. For example, the NO<sub>x</sub> emission standard changed from 0.15 g km<sup>-1</sup> to 0.035 g km<sup>-1</sup> while the standard changed from China III to China VI. Different from NO<sub>x</sub> and THC which has been controlled since China III, only when in 2017, China V standard first introduced the control of PM into the emission control scope. Yang et al. (2020) investigated the effects of gasoline upgrade policy on migrating the PM pollution in China and found that there's no much space for significantly reducing the PM concentration by simply

355 improving the gasoline quality. Therefore, for PM control, more policies i.e.  
356 developing cleaner alternatives to fossil fuels, replacing traditional vehicles with  
357 new-energy and building developed public transport system should be done.

358 The IVOC EFs for the tested China V vehicle is between the US Pre-LEV and  
359 LEV-1 vehicle. Therefore, Chinese regulations may also appear to be ineffective at  
360 controlling IVOC emissions. The IVOC-to-THC ratio measured here (0.07 for  
361 gasoline and 0.11 for E10) is higher than US vehicles (0.04), which means that IVOCs  
362 contribute a larger fraction of the THC emissions from the China V than from the US  
363 vehicles. A detailed comparison of the individual VOC emissions between China V  
364 and US LEV-2 vehicles is in SI (Figure S9).

365 UCM accounts for large fraction of IVOCs for both China V and US gasoline  
366 vehicles. However, the speciated compounds exhibit different characteristics. The  
367 China V exhaust has less speciated IVOC aromatic compounds (3.5%) and more  
368 alkanes (10.9%) compared to US exhaust (12.9% and 2.5%, respectively). This is also  
369 reflected by the IVOC mass spectrum, where Chinese vehicle exhaust has higher  $m/z$   
370 43, 57, 71, 85 signals. In addition, the specific aromatics mass fragments were not the  
371 same for China V and US IVOC emissions. For example, the dominant aromatics  
372 fragments in US gasoline exhaust are  $m/z$  128, 119, 105, 133 versus  $m/z$  135, 91, 181,  
373 189 for China V. (Fig. 2c and d).

374 Figure 3 compares the volatility distribution of the IVOC emissions from the  
375 China V and US vehicles. There are significant differences of volatility distribution  
376 between China V and US vehicles. Both distributions decrease with the increase of  
377 the retention time, but the IVOC volatility distribution of US vehicle exhaust exhibits  
378 heavier weight of lower volatility bin, i.e.  $B_{12}$  bin compared to the China V vehicle. In  
379 US exhaust the  $B_{12}$  fraction is more than double of the  $B_{13}$ . However, the contributions  
380 of  $B_{12}$ - $B_{14}$  bin volatility bins are comparable for Chinese vehicle exhaust. US vehicle  
381 exhaust has a similar IVOC volatility distribution as the unburned gasoline, indicating  
382 that the evaporate of IVOCs from fuel is non neglectable.

383 The differences between the IVOC volatility distribution between the Chinese  
384 vehicle exhaust and unburned gasoline were further investigated. The higher emission

385 factor and broader distribution of IVOCs in exhaust from China V compared with US  
386 vehicles may be due to differences in fuel composition, operating conditions and  
387 engines and after-treatment technology. As the tests of US vehicles were all  
388 performed using California commercial fuel, which is, in fact, E10 fuel. Therefore, in  
389 this study, the US (unburned) fuel or US gasoline means E10. Lu et al. (2018)  
390 demonstrated that IVOC emissions depend strongly on fuel composition. In our study,  
391 IVOCs contributed ~2.0 wt% (2.1 wt% for gasoline, 1.9 wt% for E10) of the total fuel  
392 mass, which is ~60% higher than the California fuel (E10, 1.2 wt%) (Gentner et al.,  
393 2012). Therefore, the higher IVOC fractions in China V exhaust (e.g. IVOC-to-THC  
394 ratio of 0.07 and 0.11 versus 0.04 in US exhaust) may lead to higher amounts of  
395 IVOCs in China V gasoline. When considering volatility distribution, Zhao et al.  
396 (2016) and Lu et al. (2018) reported similar distributions of IVOC between gasoline  
397 vehicle exhaust and unburned fuel, which demonstrates the significant influence of  
398 unburned fuel on exhaust volatility distribution. As a result, in Figure 3, we use US  
399 gasoline vehicle exhaust to both represent the exhaust and the unburned (E10) fuel  
400 and compare the Chinese E10 fuel with US fuel to get a comparative study. However,  
401 the volatility distribution of the China V gasoline vehicle exhaust are different from  
402 that of the unburned fuel (Figure 3). The difference might be related to the operating  
403 conditions and engine-after-treatment system.

404 Although operating conditions strongly influence the total IVOC EFs (Figure 1),  
405 Figure 3 indicates the volatility distribution of the IVOCs emissions were largely  
406 consistent across the set of test conditions. Therefore, operating conditions cannot  
407 explain the difference in the IVOC volatility distribution between the China V vehicle,  
408 unburned gasoline, and the US vehicles.

409 The engine-after-treatment system also influences IVOC emissions (Drozd et al.,  
410 2019; Alam et al., 2019; Zhao et al., 2018; Saliba et al., 2017). In order to investigate  
411 the efficiency of after-treatment system, we normalized the IVOC distributions of the  
412 fuel and exhaust to the sum of C<sub>8</sub>-C<sub>10</sub> *n*-alkanes. It is believed that the C<sub>8</sub>-C<sub>10</sub>  
413 *n*-alkanes can serve as the indicators for VOCs in fuel (Lu et al. 2018). For both US  
414 and the China V vehicles, IVOCs are enriched in the exhaust relative to the fuel.

415 However, the enrichment factor is much smaller in Chinese exhaust with a median  
 416 value of 4.0 than that for US vehicles (median value = 8.5) (Lu et al., 2018). The  
 417 enrichment factor also varies with different compounds, with the enrichment factors  
 418 of *n*-alkanes (9.3) > *b*-alkanes (6.6) > unspeciated cyclic ompounds (3.1) > aromatics  
 419 (0.4). These results are consistent with previous studies stating that the aftertreatment  
 420 devices have different removal efficiency towards different compounds (Ma et al.,  
 421 2019; Hasan et al., 2018; Hasan et al., 2016; Alam and Harrison, 2016). Our results  
 422 suggest that the Chinese three-way catalytic converter has compound dependent  
 423 efficiency (better removal of aromatics compared to alkanes) which might explain the  
 424 difference in compound composition between Chinese and US vehicle exhaust.  
 425 Furthermore, Fig. S10 shows that the catalytic converter has different removal  
 426 capacity towards different volatility bins, in which  $B_{14-16}$  works much worse compared  
 427 to other volatility bins i.e.  $B_{12}$ . Consequently, the SOA formation would be relatively  
 428 high. In sum, the compound dependent capacity and lower  $B_{14-16}$  removal efficiency  
 429 of Chinese TWC is responsible for the volatility distribution differences between  
 430 China V and US vehicles shown in Figure 3.

431 After considering all the factors above, we can draw the conclusion that fuel type,  
 432 starting mode and operating conditions can all affect the IVOCs EFs. The only factor  
 433 that impacts the volatility distribution is engine-aftertreatment system.

### 434 **3.4 Estimation of SOA Production from Chinses Vehicle Emission**

435 With the measured IVOC and VOC emissions, we estimated the SOA formation  
 436 potential by using the yield method as following (Yuan et al., 2013):

$$437 \quad \Delta\text{SOA}/\Delta\text{CO} = \sum ER_{[\text{HC}]_i} \times \left(1 - e^{- (k_{\text{OH},i} - k_{\text{CO}}) \times [\text{OH}] \times \Delta t}\right) \times Y_i$$

438 In which,  $ER_{[\text{HC}]_i}$  is the emission ratio of SOA precursor *i* ( $\text{mg kg-fuel}^{-1}$ );  $k_{\text{OH},i}$   
 439 is the OH reaction rate constant of precursor *i* at 298K ( $\text{cm}^3 \text{ molecules}^{-1} \text{ s}^{-1}$ );  $k_{\text{CO}}$  is  
 440 the OH reaction constant of CO at 298 K ( $2.4 \times 10^{-13} \text{ cm}^3 \text{ molecules}^{-1} \text{ s}^{-1}$ ); [OH] is the  
 441 OH mixing ratio, which is assumed to be  $1.5 \times 10^6 \text{ molecules cm}^3$  (Lu et al., 2019);  $\Delta t$   
 442 is photochemical age (h); and  $Y_i$  is the SOA yield determined from chamber studies.  
 443 Previous studies have shown that the SOA yield of individual hydrocarbon can be

444 influenced by  $\text{NO}_x$  level, due to the competition reactions among  $\text{RO}_2$  radicals,  $\text{NO}$   
445 and  $\text{HO}_2$  radicals. Usually SOA yields under low  $\text{NO}_x$  condition are independent on  
446 the OA loading. However, under high  $\text{NO}_x$  condition, SOA yields highly depend on  
447 OA mass concentration, which can be described using two-product or multi-products  
448 model (Presto et al., 2010; Chan et al., 2009; Ng et al., 2007). In this study, we  
449 estimated SOA formation under low and high  $\text{NO}_x$  conditions with OA concentration  
450 of 10, 20, 80  $\mu\text{g}\cdot\text{m}^{-3}$  to represent the influence of  $\text{NO}_x$  level and OA loading on SOA  
451 formation.

452 In this estimation, we include speciated  $\text{C}_6$ - $\text{C}_9$  single ring aromatics (SRAs) as  
453 typical VOCs for SOA precursors, and the corresponding  $k_{\text{OH}}$  and SOA yields are  
454 extrapolated according to two-product relationship from chamber studies (see SI) (Ng  
455 et al., 2007). The SOA yields under low and high  $\text{NO}_x$  condition, and the OH reaction  
456 rates of speciated IVOCs and SRAs are from the previous studies (see SI) (Presto et  
457 al., 2010; Lim and Ziemann, 2009; Chan et al., 2009). In brief, surrogate species were  
458 used to represent the unspciated *b*-alkanes and cyclic compounds in each of the  
459 volatility bins.

460 Figure 5 shows the POA emission and estimated SOA production under different  
461 operating conditions and  $\text{NO}_x$  level after 48 h of photo-oxidation. The estimated  
462 SOA/POA ratio is between 4.0 to 5.0 under low  $\text{NO}_x$  condition, and the SOA-to-POA  
463 ratios ranged from 1.8-2.2 to 3.8-4.4 when the OA loading increased from 10  $\mu\text{g}\cdot\text{m}^{-3}$   
464 to 80  $\mu\text{g}\cdot\text{m}^{-3}$  under high  $\text{NO}_x$  condition. The OA enhancement under low  $\text{NO}_x$   
465 condition is similar to that under high  $\text{NO}_x$  condition with the OA loading of 80  
466  $\mu\text{g}\cdot\text{m}^{-3}$ . Considering the high POA concentration and SOA formation capacity of  
467 Chinese gasoline vehicles, the SOA/POA ratios at 80  $\mu\text{g}\cdot\text{m}^{-3}$  are considered as a lower  
468 estimation. Compared with OA enhancement from US studies ( $\sim 3.6$ ) (Zhao et al.,  
469 2016), our results showed higher SOA formation potential both under low and high  
470  $\text{NO}_x$  conditions for Chinese gasoline vehicles.

471 Scenario-based analysis shows similar tendency of SOA formation potential at  
472 different OA loading under low and high  $\text{NO}_x$  condition. Though the POA emission  
473 for gasoline-fueled vehicle was higher than that fueled by E10, comparable SOA

474 formation is estimated using gasoline and E10 as fuel. That means, the OA  
475 enhancement factor for E10 is higher than that of gasoline. This suggests that  
476 although the ongoing policy of ethanol gasoline will not exacerbate the POA emission  
477 in China, the SOA formation of E10 could not be neglected due to its high SOA  
478 enhancement capacity. Therefore, more research should be done to evaluate the  
479 effectiveness of using E10 as surrogate to reduce the air pollution in China.

480 Cold-start operation has higher SOA potential with higher OA enhancement  
481 factor than hot-start, due to the higher precursors EFs caused by the reduced catalytic  
482 converter effectiveness below its light off temperature (Drozd et al., 2019). The IVOC  
483 EFs, the estimated SOA production and SOA/POA of CLTC are all higher than those  
484 of WLTC, which further demonstrates the higher SOA formation potential of Chinese  
485 gasoline vehicles under typical driving conditions in China.

486 Figure S11 presents the contribution of different classes of precursors on the  
487 SOA production after 48 h of photo-oxidation under different OA loading and NO<sub>x</sub>  
488 condition. The relative contributions of different chemical classes were similar across  
489 the different conditions, with the largest contribution from unspeciated cyclic IVOCs.  
490 This is different from the US gasoline vehicle SOA (Zhao et al., 2016) in which single  
491 ring aromatics contributes the most.

492

### 493 **3.5 Establishing the Estimation Method of SOA formation from Chinese** 494 **Gasoline Vehicles**

495 In this section, we tried to establish parameterization methods to provide simple  
496 estimations of gasoline vehicle SOA based on our measurements of VOCs and  
497 IVOCs.

498 Figure S12 shows the average predicted SOA-to-POA ratio as the function of  
499 photo-oxidation time under different OA loading and NO<sub>x</sub> conditions. In general,  
500 SOA exceeds POA after first a few hours of oxidation, and then levels off after 30 h.  
501 The SOA/POA ratio is influenced by OA concentration, NO<sub>x</sub> level and the  
502 photochemical age (OH exposure). At a certain OA loading and OH exposure,  
503 SOA/POA ratio can be estimated, and then be used to quantify the contributions of

504 gasoline vehicle SOA to the ambient OA. Therefore, we parameterized the SOA/POA  
 505 variation under different OA and NO<sub>x</sub> condition using three-parameter-based  
 506 logarithm equation, i.e.  $y=a-b \times \ln(t+c)$ , in which  $t$  represents the equivalent  
 507 photochemical age (assume that the OH concentration is  $1.5 \times 10^6$  molecules cm<sup>3</sup>) and  
 508 a, b, c can be described using three-parameter logarithm equation  $y=m-n \times \ln([\text{OA}$   
 509 concentration]+p). Table 1 shows the parameterization results of compounds-based  
 510 SOA/POA variation under the different OA and NO<sub>x</sub> condition. The fits quality could  
 511 be found in Figure S13.

512 Table 1 Coefficient of parameterization between SOA/POA and photochemical age

| SOA/POA          | Low NO <sub>x</sub> condition | High NO <sub>x</sub> condition |         |        |
|------------------|-------------------------------|--------------------------------|---------|--------|
|                  |                               | m                              | n       | p      |
| a                | -0.62                         | 0.46                           | 0.22    | 9.8    |
| b                | -1.34                         | 0.27                           | 0.33    | 2.58   |
| c                | 0.58                          | 0.13                           | -0.09   | 3.35   |
| Unspeciated      |                               |                                |         |        |
| cyclic compounds |                               |                                |         |        |
| a                | -0.15                         | 0.26                           | 0.09    | 21.76  |
| b                | -0.72                         | 0.086                          | 0.18    | 0.46   |
| c                | 0.11                          | -0.278                         | -0.083  | 24.42  |
| Unspeciated      |                               |                                |         |        |
| b-alkanes        |                               |                                |         |        |
| a                | -0.11                         | 0.47                           | 0.111   | 87.54  |
| b                | -0.17                         | 0.15                           | 0.070   | 12.36  |
| c                | 0.84                          | -0.17                          | -0.21   | 41.97  |
| aromatics        |                               |                                |         |        |
| a                | -0.03                         | -0.023                         | -0.0098 | 40.52  |
| b                | -0.03                         | 0.012                          | 0.007   | 17.27  |
| c                | -1.00                         | -1.02                          | -0.021  | -10.00 |
| n-alkanes        |                               |                                |         |        |
| a                | -0.05                         | 0.0067                         | 0.013   | -2.38  |
| b                | -0.11                         | 0.019                          | 0.030   | -0.52  |
| c                | 0.48                          | 0.15                           | -0.058  | 29.18  |
| Single ring      |                               |                                |         |        |

| aromatics |       |      |       |       |
|-----------|-------|------|-------|-------|
| a         | -0.51 | 0.28 | 0.17  | 5.47  |
| b         | -0.35 | 0.03 | 0.059 | -2.29 |
| c         | 3.92  | 2.80 | -1.29 | 10.84 |

513 The above photochemical-based parameterization method provides a conservative  
514 way to quantify the evolution of SOA from Chinese gasoline vehicle VOCs and  
515 IVOCs oxidation. However, there are still some uncertainties which may lead to  
516 discrepancies between predicted and measured SOA. In general, positive or negative  
517 artifacts of quartz filters, *n*-alkane equivalent method in estimating the IVOCs  
518 concentration, uncertainty in SOA yield, surrogate method to substitute SOA yield  
519 and  $k_{OH}$  for UCM and lack of semi-volatile organic compounds will exert influence on  
520 the SOA prediction.

521

#### 522 **4 Atmospheric Implications**

523 We measured the VOCs, IVOCs and POA emitted from a China V light duty  
524 gasoline vehicle across a wide range of operating conditions. Compared with US  
525 LEV-2 gasoline vehicles, the China V vehicle emits three times more IVOCs. Besides,  
526 the IVOC emissions from the China V vehicle have a much broader volatility  
527 distribution than that from US vehicles. These characteristics imply that IVOCs could  
528 act more important SOA precursors in China than those in the US. For Chinese  
529 gasoline vehicles, although the magnitude of the emission of IVOCs and VOCs can  
530 vary, their relative contribution to SOA production is similar across the set of  
531 operating conditions examined here due to the similar volatility distributions. As a  
532 result, the key to control SOA formation of gasoline vehicles is to reduce the total  
533 IVOC EFs by upgrading of emissions controls. In addition, reducing congestion and  
534 other low speed operating modes would also be effective at reducing emissions  
535 (Figure 1 and 5).

536 Based on our results, we roughly estimate the vehicle IVOC emissions in China.  
537 Till the end of 2018, the total vehicle population in China reached 0.327 billion, with  
538 automobiles contributing 61% (0.24 billion). Of all the automobiles, gasoline-fueled

539 car took the dominant (88.1%). The HC emission of gasoline vehicles in China was  
540 0.23 Mt, accounting for more than 70% of the total vehicle emissions. Using an  
541 IVOC/THC ratio of 0.09 that is obtained in our work, we estimate that the vehicle  
542 IVOC emissions in China are 0.03 Mt (30 Gg), in which 20 Gg is attributed to  
543 gasoline vehicles. One should note that this estimation is a conservative value, since  
544 we consider all vehicles as gasoline vehicles, and all of them meet the China V  
545 standard. According to the statistics from the Ministry of Ecology and Environment,  
546 only 30.9% of the vehicles in 2018 meet the standards of China V. Indeed, higher  
547 percentage of pre-China V e.g. China I-IV standard cars will cause more IVOCs  
548 emission. In addition, the IVOC/NMHC ratio of diesel vehicles could be much higher  
549 than that of the gasoline vehicles (Zhao et al., 2016, 2015). This may also lead to an  
550 underestimation.

551 Our results show that using a Chinese real-world test protocol CLTC will result  
552 in substantially higher IVOC emissions compared with WLTC which might have  
553 close relationship with frequent idling and low acceleration condition. Therefore,  
554 when driving at typical Chinese condition where traffic congestion frequently occur,  
555 the IVOCs emission from Chinese gasoline vehicles would be much higher than the  
556 current limited emission inventory. Our results indicate simply controlling the THC,  
557 NO<sub>x</sub> and primary PM emissions may be insufficient in the aspect of controlling  
558 particle pollution. Reducing IVOC emissions should also be taken into consideration  
559 due to their high contribution to SOA formation, which is more important than  
560 primary organic aerosol. Suggested controlling ways include upgrading the fuel  
561 quality and engine-after treatment system, and reducing the traffic congestion.

562 Though we have discussed the influences of different operating conditions on  
563 IVOC emissions and SOA formation for the tested China V gasoline vehicle, due to  
564 the singular vehicle tests of our study, more research i.e. vehicles meeting different  
565 emission standards, different engines should be performed both to testify the accuracy  
566 of our research and to get a full understanding of the IVOC emission inventory for  
567 Chinese gasoline vehicles. Furthermore, advanced measurement techniques e.g. GC×  
568 GC-MS and chemical ionization mass spectrometry (CIMS) should be used to obtain

569 a comprehensive molecular-level picture of the total organics so as to reduce the  
570 uncertainties associated with the measurements and models.

571

### 572 ***Data availability***

573 The data used in this publication are available on  
574 <https://doi.org/10.5281/zenodo.4072847>, and they can be accessed by request to the  
575 corresponding author ([songguo@pku.edu.cn](mailto:songguo@pku.edu.cn)) of Peking University. The IVOCs  
576 emissions from US vehicles used in this study can be accessed via  
577 <https://pubs.acs.org/doi/abs/10.1021/acs.est.5b06247> (Zhao et al., 2016) and  
578 <https://acp.copernicus.org/articles/18/17637/2018/> (Lu et al, 2018). The primary  
579 emissions and fuel compositions from US vehicles used in this study can be accessed  
580 via <https://www.sciencedirect.com/science/article/pii/S1352231014000715> (May et al.,  
581 2014).

582

### 583 ***Competing interests***

584 The authors declare that they have no conflict of interest.

585

### 586 ***Author contributions***

587 SG, RZ and HW designed the study. RZ and KS collected the samples. RZ and QL  
588 analyzed the samples and processed the data. RZ wrote the paper, with contributions  
589 from all the coauthors.

590

### 591 ***Acknowledgement***

592 This research is supported by the National Key Research and Development Program  
593 of China (2016YFC0202000), the National Natural Science Foundation of China (No.  
594 51636003, 41977179, 21677002, 91844301), Beijing Municipal Science and  
595 Technology Commission (Z201100008220011), and Natural Science Foundation of  
596 Beijing (No. 8192022), the Open Research Fund of State Key Laboratory of  
597 Multi-phase Complex Systems (MPCS-2019-D-09). ALR and QY received financial  
598 support from the Center for Air, Climate, and Energy Solutions (CACES), which was  
599 funded by Assistance Agreement No. RD83587301 awarded by the U.S.  
600 Environmental Protection Agency. It has not been formally reviewed by EPA. The

601 views expressed in this document are solely those of authors and do not necessarily  
602 reflect those of the Agency. EPA does not endorse any products or commercial  
603 services mentioned in this publication.

604

## 605 **References**

606 Alam, M. S., and Harrison, R. M.: Recent advances in the application of 2-dimensional gas  
607 chromatography with soft and hard ionisation time-of-flight mass spectrometry in environmental  
608 analysis, *Chemical Science*, 7, 3968-3977, 10.1039/c6sc00465b, 2016.

609 Alam, M. S., Zeraati-Rezaei, S., Xu, H., and Harrison, R. M.: Characterization of Gas and Particulate  
610 Phase Organic Emissions (C9–C37) from a Diesel Engine and the Effect of Abatement Devices,  
611 *Environmental science & technology*, 53, 11345-11352, 2019.

612 Cao, X., Yao, Z., Shen, X., Ye, Y., and Jiang, X.: On-road emission characteristics of VOCs from  
613 light-duty gasoline vehicles in Beijing, China, *Atmospheric Environment*, 124, 146-155,  
614 <https://doi.org/10.1016/j.atmosenv.2015.06.019>, 2016.

615 Chan, A. W. H., Kautzman, K. E., Chhabra, P. S., Surratt, J. D., Chan, M. N., Crounse, J. D., Kuerten,  
616 A., Wennberg, P. O., Flagan, R. C., and Seinfeld, J. H.: Secondary organic aerosol formation from  
617 photooxidation of naphthalene and alkylnaphthalenes: implications for oxidation of intermediate  
618 volatility organic compounds (IVOCs), *Atmospheric Chemistry and Physics*, 9, 3049-3060,  
619 10.5194/acp-9-3049-2009, 2009.

620 Cross, E. S., Sappok, A. G., Wong, V. W., and Kroll, J. H.: Load-Dependent Emission Factors and  
621 Chemical Characteristics of IVOCs from a Medium-Duty Diesel Engine, *Environmental Science &  
622 Technology*, 49, 13483-13491, 10.1021/acs.est.5b03954, 2015.

623 Dall'Osto, M., Harrison, R., Coe, H., and Williams, P.: Real-time secondary aerosol formation during a  
624 fog event in London, *Atmospheric Chemistry and Physics*, 9, 2459-2469, 2009.

625 Donahue, N. M., Robinson, A. L., Stanier, C. O., and Pandis, S. N.: Coupled partitioning, dilution, and  
626 chemical aging of semivolatile organics, *Environ. Sci. Technol.*, 40, 2635-2643, Doi  
627 10.1021/Es052297c, 2006.

628 Drozd, G. T., Zhao, Y., Saliba, G., Frodin, B., Maddox, C., Weber, R. J., Chang, M. C. O., Maldonado,  
629 H., Sardar, S., Robinson, A. L., and Goldstein, A. H.: Time Resolved Measurements of Speciated  
630 Tailpipe Emissions from Motor Vehicles: Trends with Emission Control Technology, Cold Start  
631 Effects, and Speciation, *Environmental Science & Technology*, 50, 13592-13599,  
632 10.1021/acs.est.6b04513, 2016.

633 Drozd, G. T., Zhao, Y., Saliba, G., Frodin, B., Maddox, C., Chang, M. C. O., Maldonado, H., Sardar, S.,  
634 Weber, R. J., Robinson, A. L., and Goldstein, A. H.: Detailed speciation of intermediate volatility  
635 and semivolatile organic compound emissions from gasoline vehicles: effects of cold starts and  
636 implications for secondary organic aerosol formation, *Environmental Science & Technology*, 53,  
637 1706-1714, 10.1021/acs.est.8b05600, 2019.

638 Fontaras, G., Franco, V., Dilara, P., Martini, G., and Manfredi, U.: Development and review of Euro 5  
639 passenger car emission factors based on experimental results over various driving cycles, *Science of  
640 The Total Environment*, 468-469, 1034-1042, <https://doi.org/10.1016/j.scitotenv.2013.09.043>, 2014.

641 Gentner, D. R., Isaacman, G., Worton, D. R., Chan, A. W. H., Dallmann, T. R., Davis, L., Liu, S., Day,  
642 D. A., Russell, L. M., Wilson, K. R., Weber, R., Guha, A., Harley, R. A., and Goldstein, A. H.:  
643 Elucidating secondary organic aerosol from diesel and gasoline vehicles through detailed

644 characterization of organic carbon emissions, *Proceedings of the National Academy of Sciences of*  
645 *the United States of America*, 109, 18318-18323, 2012.

646 Giani, P., Balzarini, A., Pirovano, G., Gilardoni, S., Paglione, M., Colombi, C., Gianelle, V. L., Belis, C.  
647 A., Poluzzi, V., and Lonati, G.: Influence of semi- and intermediate-volatile organic compounds  
648 (S/IVOC) parameterizations, volatility distributions and aging schemes on organic aerosol  
649 modelling in winter conditions, *Atmospheric Environment*, 213, 11-24,  
650 10.1016/j.atmosenv.2019.05.061, 2019.

651 Guo, S., Hu, M., Wang, Z. B., Slanina, J., and Zhao, Y. L.: Size-resolved aerosol water-soluble ionic  
652 compositions in the summer of Beijing: implication of regional secondary formation, *Atmospheric*  
653 *Chemistry and Physics*, 10, 947-959, 2010.

654 Guo, S., Hu, M., Guo, Q., Zhang, X., Schauer, J. J., and Zhang, R.: Quantitative evaluation of emission  
655 controls on primary and secondary organic aerosol sources during Beijing 2008 Olympics,  
656 *Atmospheric Chemistry and Physics*, 13, 8303-8314, 2012a.

657 Guo, S., Hu, M., Guo, Q. F., Zhang, X., Zheng, M., Zheng, J., Chang, C. C., Schauer, J. J., and Zhang,  
658 R. Y.: Primary Sources and Secondary Formation of Organic Aerosols in Beijing, China,  
659 *Environmental Science & Technology*, 46, 9846-9853, 10.1021/es20425641, 2012b.

660 Guo, S., Hu, M., Shang, D. J., Guo, Q. F., and Hu, W. W.: Research on Secondary Organic Aerosols  
661 Basing on Field Measurement, *Acta Chim Sinica*, 72, 145-157, 10.6023/A13111169, 2014a.

662 Guo, S., Hu, M., Zamora, M. L., Peng, J. F., Shang, D. J., Zheng, J., Du, Z. F., Wu, Z., Shao, M., Zeng,  
663 L. M., Molina, M. J., and Zhang, R. Y.: Elucidating severe urban haze formation in China, *P Natl*  
664 *Acad Sci USA*, 111, 17373-17378, 2014b.

665 Guo, S., Hu, M., Lin, Y., Gomez-Hernandez, M., Zamora, M. L., Peng, J. F., Collins, D. R., and Zhang,  
666 R. Y.: OH-Initiated Oxidation of m-Xylene on Black Carbon Aging, *Environ. Sci. Technol.*, 50,  
667 8605-8612, 10.1021/acs.est.6b01272, 2016.

668 Guo, S., Hu, M., Peng, J., Wu, Z., Zamora, M. L., Shang, D., Du, Z., Zheng, J., Fang, X., Tang, R., Wu,  
669 Y., Zeng, L., Shuai, S., Zhang, W., Wang, Y., Ji, Y., Li, Y., Zhang, A. L., Wang, W., Zhang, F., Zhao,  
670 J., Gong, X., Wang, C., Molina, M. J., and Zhang, R.: Remarkable nucleation and growth of  
671 ultrafine particles from vehicular exhaust, *P Natl Acad Sci USA*, 117, 3427-3432,  
672 10.1073/pnas.1916366117, 2020.

673 Hallquist, M., Wenger, J. C., Baltensperger, U., Rudich, Y., Simpson, D., Claeys, M., Dommen, J.,  
674 Donahue, N. M., George, C., Goldstein, A. H., Hamilton, J. F., Herrmann, H., Hoffmann, T., Iinuma,  
675 Y., Jang, M., Jenkin, M. E., Jimenez, J. L., Kiendler-Scharr, A., Maenhaut, W., McFiggans, G.,  
676 Mentel, T. F., Monod, A., Prevot, A. S. H., Seinfeld, J. H., Surratt, J. D., Szmigielski, R., and Wildt,  
677 J.: The formation, properties and impact of secondary organic aerosol: current and emerging issues,  
678 *Atmos. Chem. Phys.*, 9, 5155-5236, 2009.

679 Hallquist, M., Munthe, J., Hu, M., Wang, T., Chan, C. K., Gao, J., Boman, J., Guo, S., Hallquist, A. M.,  
680 and Mellqvist, J.: Photochemical smog in China: scientific challenges and implications for  
681 air-quality policies, *National Science Review*, 3, 401-403, 2016.

682 Hasan, A. O., Abu-jrai, A., Al-Muhtaseb, A. a. H., Tsolakis, A., and Xu, H.: Formaldehyde,  
683 acetaldehyde and other aldehyde emissions from HCCI/SI gasoline engine equipped with prototype  
684 catalyst, *Fuel*, 175, 249-256, <https://doi.org/10.1016/j.fuel.2016.02.005>, 2016.

685 Hasan, A. O., Elghawi, U. M., Al-Muhtaseb, A. a. H., Abu-jrai, A., Al-Rawashdeh, H., and Tsolakis, A.:  
686 Influence of composite after-treatment catalyst on particle-bound polycyclic aromatic  
687 hydrocarbons–vapor-phase emitted from modern advanced GDI engines, *Fuel*, 222, 424-433,

688 <https://doi.org/10.1016/j.fuel.2018.02.114>, 2018.

689 Hu, M., Guo, S., Peng, J., and Wu, Z.: Insight into characteristics and sources of PM<sub>2.5</sub> in the Beijing–  
690 Tianjin–Hebei region, China, *National Science Review*, 2, 257-258, 2015.

691 Huang, C., Wang, H., Li, L., Wang, Q., Lu, Q., De Gouw, J., Zhou, M., Jing, S., Lu, J., and Chen, C.:  
692 VOC species and emission inventory from vehicles and their SOA formation potentials estimation  
693 in Shanghai, China, *Atmospheric Chemistry and Physics*, 15, 11081-11096, 2015.

694 Huang, C., Hu, Q., Li, Y., Tian, J., Ma, Y., Zhao, Y., Feng, J., An, J., Qiao, L., Wang, H., Jing, S. a.,  
695 Huang, D., Lou, S., Zhou, M., Zhu, S., Tao, S., and Li, L.: Intermediate Volatility Organic  
696 Compound Emissions from a Large Cargo Vessel Operated under Real-world Conditions,  
697 *Environmental Science & Technology*, 52, 12934-12942, 10.1021/acs.est.8b04418, 2018.

698 Huang, G., Liu, Y., Shao, M., Li, Y., Chen, Q., Zheng, Y., Wu, Z., Liu, Y., Wu, Y., and Hu, M.:  
699 Potentially Important Contribution of Gas-Phase Oxidation of Naphthalene and Methyl-naphthalene  
700 to Secondary Organic Aerosol during Haze Events in Beijing, *Environmental Science &  
701 Technology*, 53, 1235-1244, 2019.

702 Huang, L., Wang, Q., Wang, Y., Emery, C., Zhu, A., Zhu, Y., Yin, S., Yarwood, G., Zhang, K., and Li,  
703 L.: Simulation of secondary organic aerosol over the Yangtze River Delta region: The impacts from  
704 the emissions of intermediate volatility organic compounds and the SOA modeling framework,  
705 *Atmospheric Environment*, 118079, 10.1016/j.atmosenv.2020.118079, 2020.

706 Jaworski, A., Kuszewski, H., Ustrzycki, A., Balawender, K., Lejda, K., and Woś, P.: Analysis of the  
707 repeatability of the exhaust pollutants emission research results for cold and hot starts under  
708 controlled driving cycle conditions, *Environmental Science and Pollution Research*, 25,  
709 17862-17877, 10.1007/s11356-018-1983-5, 2018.

710 Koo, B., Knipping, E., and Yarwood, G.: 1.5-Dimensional volatility basis set approach for modeling  
711 organic aerosol in CAMx and CMAQ, *Atmospheric Environment*, 95, 158-164,  
712 <https://doi.org/10.1016/j.atmosenv.2014.06.031>, 2014.

713 Lim, Y. B., and Ziemann, P. J.: Effects of molecular structure on aerosol yields from OH  
714 radical-initiated reactions of linear, branched, and cyclic alkanes in the presence of NO<sub>x</sub>,  
715 *Environmental science & technology*, 43, 2328-2334, 2009.

716 Lu, K., Guo, S., Tan, Z., Wang, H., Shang, D., Liu, Y., Li, X., Wu, Z., Hu, M., and Zhang, Y.: Exploring  
717 atmospheric free-radical chemistry in China: the self-cleansing capacity and the formation of  
718 secondary air pollution, *National Science Review*, 6, 579-594, 2019.

719 Lu, Q., Zhao, Y., and Robinson, A. L.: Comprehensive organic emission profiles for gasoline, diesel,  
720 and gas-turbine engines including intermediate and semi-volatile organic compound emissions,  
721 *Atmospheric Chemistry and Physics*, 18, 17637-17654, 2018.

722 Ma, R., He, X., Zheng, Y., Zhou, B., Lu, S., and Wu, Y.: Real-world driving cycles and energy  
723 consumption informed by large-sized vehicle trajectory data, *Journal of Cleaner Production*, 223,  
724 564-574, <https://doi.org/10.1016/j.jclepro.2019.03.002>, 2019.

725 Marotta, A., Pavlovic, J., Ciuffo, B., Serra, S., and Fontaras, G.: Gaseous Emissions from Light-Duty  
726 Vehicles: Moving from NEDC to the New WLTP Test Procedure, *Environmental Science &  
727 Technology*, 49, 8315-8322, 10.1021/acs.est.5b01364, 2015.

728 May, A. A., Nguyen, N. T., Presto, A. A., Gordon, T. D., Lipsky, E. M., Karve, M., Gutierrez, A.,  
729 Robertson, W. H., Zhang, M., Brandow, C., Chang, O., Chen, S. Y., Cicero-Fernandez, P., Dinkins,  
730 L., Fuentes, M., Huang, S. M., Ling, R., Long, J., Maddox, C., Massetti, J., McCauley, E., Miguel,  
731 A., Na, K., Ong, R., Pang, Y. B., Rieger, P., Sax, T., Truong, T., Vo, T., Chattopadhyay, S.,

732 Maldonado, H., Maricq, M. M., and Robinson, A. L.: Gas- and particle-phase primary emissions  
733 from in-use, on-road gasoline and diesel vehicles, *Atmospheric Environment*, 88, 247-260, 2014.

734 Murphy, B. N., Woody, M. C., Jimenez, J. L., Carlton, A. M. G., and Pye, H. O. T.: Semivolatile POA  
735 and parameterized total combustion SOA in CMAQv5.2: impacts on source strength and  
736 partitioning, *Atmospheric Chemistry & Physics*, 17, 11107-11133, 2017.

737 Ng, N., Kroll, J., Chan, A., Chhabra, P., Flagan, R., and Seinfeld, J.: Secondary organic aerosol  
738 formation from m-xylene, toluene, and benzene, *Atmospheric Chemistry and Physics*, 7, 3909-3922,  
739 2007.

740 Peng, J. F., Hu, M., Guo, S., Du, Z. F., Zheng, J., Shang, D. J., Zamora, M. L., Zeng, L. M., Shao, M.,  
741 Wu, Y. S., Zheng, J., Wang, Y., Glen, C. R., Collins, D. R., Molina, M. J., and Zhang, R. Y.:  
742 Markedly enhanced absorption and direct radiative forcing of black carbon under polluted urban  
743 environments, *P Natl Acad Sci USA*, 113, 4266-4271, 10.1073/pnas.1602310113, 2016.

744 Peng, J. F., Hu, M., Du, Z. F., Wang, Y. H., Zheng, J., Zhang, W. B., Yang, Y. D., Qin, Y. H., Zheng, R.,  
745 Xiao, Y., Wu, Y. S., Lu, S. H., Wu, Z. J., Guo, S., Mao, H. J., and Shuai, S. J.: Gasoline aromatics: a  
746 critical determinant of urban secondary organic aerosol formation, *Atmospheric Chemistry and  
747 Physics*, 17, 10743-10752, 10.5194/acp-17-10743-2017, 2017.

748 Presto, A. A., Miracolo, M. A., Donahue, N. M., and Robinson, A. L.: Secondary organic aerosol  
749 formation from high-NO(x) photo-oxidation of low volatility precursors: n-alkanes, *Environmental  
750 Science & Technology*, 44, 2029-2034, 2010.

751 Pretsch, E., Clerc, T., Seibl, J., and Simon, W.: *Tables of spectral data for structure determination of  
752 organic compounds*, Springer Science & Business Media, 2013.

753 Qi, L., Liu, H., Shen, X. e., Fu, M., Huang, F., Man, H., Deng, F., Shaikh, A. A., Wang, X., Dong, R.,  
754 Song, C., and He, K.: Intermediate-Volatility Organic Compound Emissions from Nonroad  
755 Construction Machinery under Different Operation Modes, *Environmental Science & Technology*,  
756 53, 13832-13840, 10.1021/acs.est.9b01316, 2019.

757 Robinson, A. L., Donahue, N. M., Shrivastava, M. K., Weitkamp, E. A., Sage, A. M., Grieshop, A. P.,  
758 Lane, T. E., Pierce, J. R., and Pandis, S. N.: Rethinking Organic Aerosols: Semivolatile Emissions  
759 and Photochemical Aging, *Science*, 315, 1259-1262, 2007.

760 Saliba, G., Saleh, R., Zhao, Y., Presto, A. A., Larnbe, A. T., Frodin, B., Sardar, S., Maldonado, H.,  
761 Maddox, C., May, A. A., Drozd, G. T., Goldstein, A. H., Russell, L. M., Hagen, F., and Robinson, A.  
762 L.: Comparison of Gasoline Direct-Injection (GDI) and Port Fuel Injection (PFI) Vehicle Emissions:  
763 Emission Certification Standards, Cold-Start, Secondary Organic Aerosol Formation Potential, and  
764 Potential Climate Impacts, *Environmental Science & Technology*, 51, 6542-6552,  
765 10.1021/acs.est.6b06509, 2017.

766 Spencer, M. T., Shields, L. G., Sodeman, D. A., Toner, S. M., and Prather, K. A.: Comparison of oil and  
767 fuel particle chemical signatures with particle emissions from heavy and light duty vehicles,  
768 *Atmospheric Environment*, 40, 5224-5235, 2006.

769 Suarez-Bertoa, R., Zardini, A. A., Keuken, H., and Astorga, C.: Impact of ethanol containing gasoline  
770 blends on emissions from a flex-fuel vehicle tested over the Worldwide Harmonized Light duty Test  
771 Cycle (WLTC), *Fuel*, 143, 173-182, <https://doi.org/10.1016/j.fuel.2014.10.076>, 2015.

772 Tang, R., Wang, H., Liu, Y., and Guo, S.: Constituents of Atmospheric Semi-Volatile and Intermediate  
773 Volatility Organic Compounds and Their Contribution to Organic Aerosol, *Prog Chem*, 31, 180-190,  
774 10.7536/PC180431, 2019.

775 Tang, R. Z., Wu, Z. P., Li, X., Wang, Y. J., Shang, D. J., Xiao, Y., Li, M. R., Zeng, L. M., Wu, Z. J.,

776 Hallquist, M., Hu, M., and Guo, S.: Primary and secondary organic aerosols in summer 2016 in  
777 Beijing, *Atmos. Chem. Phys.*, 18, 4055-4068, 10.5194/acp-18-4055-2018, 2018.

778 Wang, H., Yu, Y., Tang, R., and Guo, S.: Research on Formation and Aging of Secondary Organic  
779 Aerosol Based on Simulation Methods, *Acta Chim Sinica*, 78, 516-527, 10.6023/A20020036, 2020.

780 Woody, M. C., Wong, H. W., West, J. J., and Arunachalam, S.: Multiscale predictions of  
781 aviation-attributable PM<sub>2.5</sub> for US airports modeled using CMAQ with plume-in-grid and an  
782 aircraft-specific 1-D emission model, *Atmospheric Environment*, 147, 384-394,  
783 10.1016/j.atmosenv.2016.10.016, 2016.

784 Wu, Y., Zhang, S., Hao, J., Liu, H., Wu, X., Hu, J., Walsh, M. P., Wallington, T. J., Zhang, K. M., and  
785 Stevanovic, S.: On-road vehicle emissions and their control in China: A review and outlook,  
786 *Science of The Total Environment*, 574, 332-349, 2017.

787 Yang, G., Zhang, Y., and Li, X.: Impact of gasoline upgrade policy on particulate matter pollution in  
788 China, *Journal of Cleaner Production*, 262, 121336, 10.1016/j.jclepro.2020.121336, 2020.

789 Yu, Y., Wang, H., Wang, T., Song, K., Tan, T., Wan, Z., Gao, Y., Dong, H., Chen, S., Zeng, L., Hu, M.,  
790 Wang, H., Lou, S., Zhu, W., and Guo, S.: Elucidating the importance of semi-volatile organic  
791 compounds to secondary organic aerosol formation at a regional site during the EXPLORE-YRD  
792 campaign, *Atmos. Environ.*, 10.1016/j.atmosenv.2020.118043, 2020.

793 Yuan, B., Hu, W. W., Shao, M., Wang, M., Chen, W. T., Lu, S. H., Zeng, L. M., and Hu, M.: VOC  
794 emissions, evolutions and contributions to SOA formation at a receptor site in eastern China, *Atmos.*  
795 *Chem. Phys.*, 13, 8815-8832, 10.5194/acp-13-8815-2013, 2013.

796 Zhang, Q., Jimenez, J., Canagaratna, M., Allan, J., Coe, H., Ulbrich, I., Alfarra, M., Takami, A.,  
797 Middlebrook, A., and Sun, Y.: Ubiquity and dominance of oxygenated species in organic aerosols in  
798 anthropogenically - influenced Northern Hemisphere midlatitudes, *Geophysical Research Letters*,  
799 34, 2007.

800 Zhang, S., Wu, Y., Wu, X., Li, M., Ge, Y., Liang, B., Xu, Y., Zhou, Y., Liu, H., Fu, L., and Hao, J.:  
801 Historic and future trends of vehicle emissions in Beijing, 1998–2020: A policy assessment for the  
802 most stringent vehicle emission control program in China, *Atmospheric Environment*, 89, 216-229,  
803 <https://doi.org/10.1016/j.atmosenv.2013.12.002>, 2014.

804 Zhao, Y., Hennigan, C. J., May, A. A., Tkacik, D. S., de Gouw, J. A., Gilman, J. B., Kuster, W. C.,  
805 Borbon, A., and Robinson, A. L.: Intermediate-Volatility Organic Compounds: A Large Source of  
806 Secondary Organic Aerosol, *Environmental Science & Technology*, 48, 13743-13750,  
807 10.1021/es5035188, 2014.

808 Zhao, Y., Nguyen, N. T., Presto, A. A., Hennigan, C. J., May, A. A., and Robinson, A. L.: Intermediate  
809 Volatility Organic Compound Emissions from On-Road Diesel Vehicles: Chemical Composition,  
810 Emission Factors, and Estimated Secondary Organic Aerosol Production, *Environmental Science &*  
811 *Technology*, 49, 11516-11526, 10.1021/acs.est.3b02841, 2015.

812 Zhao, Y., Nguyen, N. T., Presto, A. A., Hennigan, C. J., May, A. A., and Robinson, A. L.: Intermediate  
813 Volatility Organic Compound Emissions from On-Road Gasoline Vehicles and Small Off-Road  
814 Gasoline Engines, *Environmental Science & Technology*, 50, 4554-4563, 10.1021/acs.est.5b06247,  
815 2016.

816 Zhao, Y., Lambe, A. T., Saleh, R., Saliba, G., and Robinson, A. L.: Secondary organic aerosol  
817 production from gasoline vehicle exhaust: Effects of engine technology, cold start, and emission  
818 certification standard, *Environmental science & technology*, 52, 1253-1261, 2018.

819

820 **Figure Caption**

821 **Figure 1.** IVOC emission factors measured under different conditions, i.e. different  
822 fuel type (gasoline, E10), test cycles (Chinese Light vehicles Test Cycle, CLTC,  
823 and World-wide harmonized Light-duty Test Cycle, WLTC), starting mode (hot  
824 start and cold start), and acceleration rates (acceleration rates of 1.2, 3.6 and 6.0  
825 km/h/s). Stars indicate the EF data from US, i.e. median US LEV-2 gasoline  
826 vehicles (vehicles manufactured in 2004-2012), non-road construction machinery,  
827 and a large cargo vessel (Qi et al., 2019;Huang et al., 2018;Zhao et al., 2016). The  
828 first category “China V” is the compilation of all the EF results from all of the  
829 CLTC and WLTC tests. The boxes indicate the median value, with error bars  
830 represent one standard deviation.

831 **Figure 2.** (a) Comparison of average chemical speciation of IVOC emissions from  
832 China V vehicle and US vehicles (Zhao et al., 2016); (b) Average mass spectrum  
833 of the IVOC during a typical E10-fueled cold start CLTC test. (c-d) Box-whisker  
834 plots of the fractional contribution of selected fragments to total IVOCs signal for  
835 tested China V vehicle: (c)  $B_{12}$ - $B_{16}$  bins; (d)  $B_{17}$ - $B_{22}$  bins. The boxes represent the  
836 25<sup>th</sup> and 75<sup>th</sup> percentiles with the centerline being the median. The whiskers are the  
837 10<sup>th</sup> and 90<sup>th</sup> percentiles. Black hollow triangles represent median LEV-2 data  
838 from Zhao et al. <sup>13</sup> LEV-2 represents vehicles manufactured from 2004 to 2012.  
839 Fragments colored in blue represent aliphatic compounds, while those colored in  
840 orange are associated with aromatic compounds.

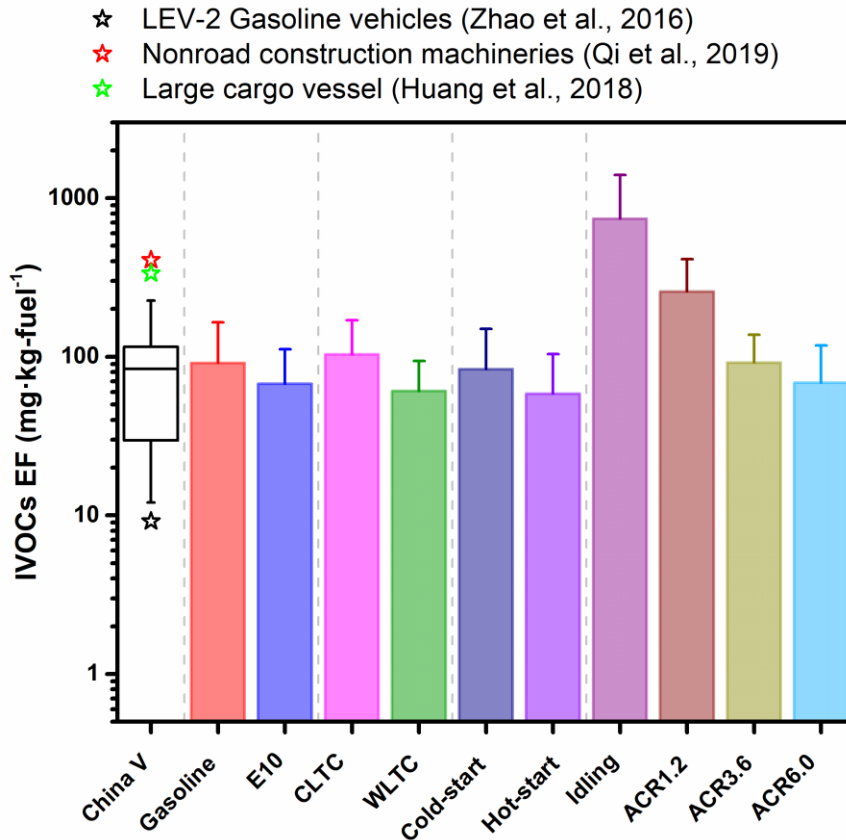
841 **Figure 3.** Comparison of IVOC volatility distributions of Chinses gasoline vehicle  
842 exhaust, US gasoline vehicle exhaust, and Chinses E10 fuel. The box-plot  
843 represents the Chinses gasoline vehicle exhaust. The boxes represent the 25<sup>th</sup> and  
844 75<sup>th</sup> percentiles with the centerline being the median. The whiskers are the 10<sup>th</sup> and  
845 90<sup>th</sup> percentiles. Red solid circles represent IVOC fractions of US vehicle exhaust  
846 (Zhao et al., 2016). Blue hollow triangles represent the IVOCs volatility  
847 distribution of Chinese E10 fuel. As all the studies performed in US used  
848 commercial US gasoline as fuel, which contained 10% v/v ethanol, i.e. E10 fuel.  
849 Therefore, we compare the Chinese E10 with US fuel to get a consistent

850 comparison. Also, we should note that Zhao et al. (2016) and Lu et al. (2018)  
851 found that consistent distribution of US fuel and exhaust, so in this figure, the US  
852 gasoline vehicle exhaust can represent the volatility distribution of its unburned  
853 fuel distribution as well.

854 **Figure 4.** Comparison of emission factors of (a) PM (b) NO<sub>x</sub> (c) THC, and (d) IVOC  
855 between China and US on road gasoline vehicles (Zhao et al., 2016; May et al.,  
856 2014). The boxes present the 75<sup>th</sup> and 25<sup>th</sup> percentiles with the centerline  
857 represents being the median. The US vehicles are grouped by the model year, i.e.  
858 pre-LEV refers to vehicles manufactured prior to 1994, LEV-1 represents vehicles  
859 from 1994-2003, and LEV-2 is vehicles manufactured from 2004-2012.

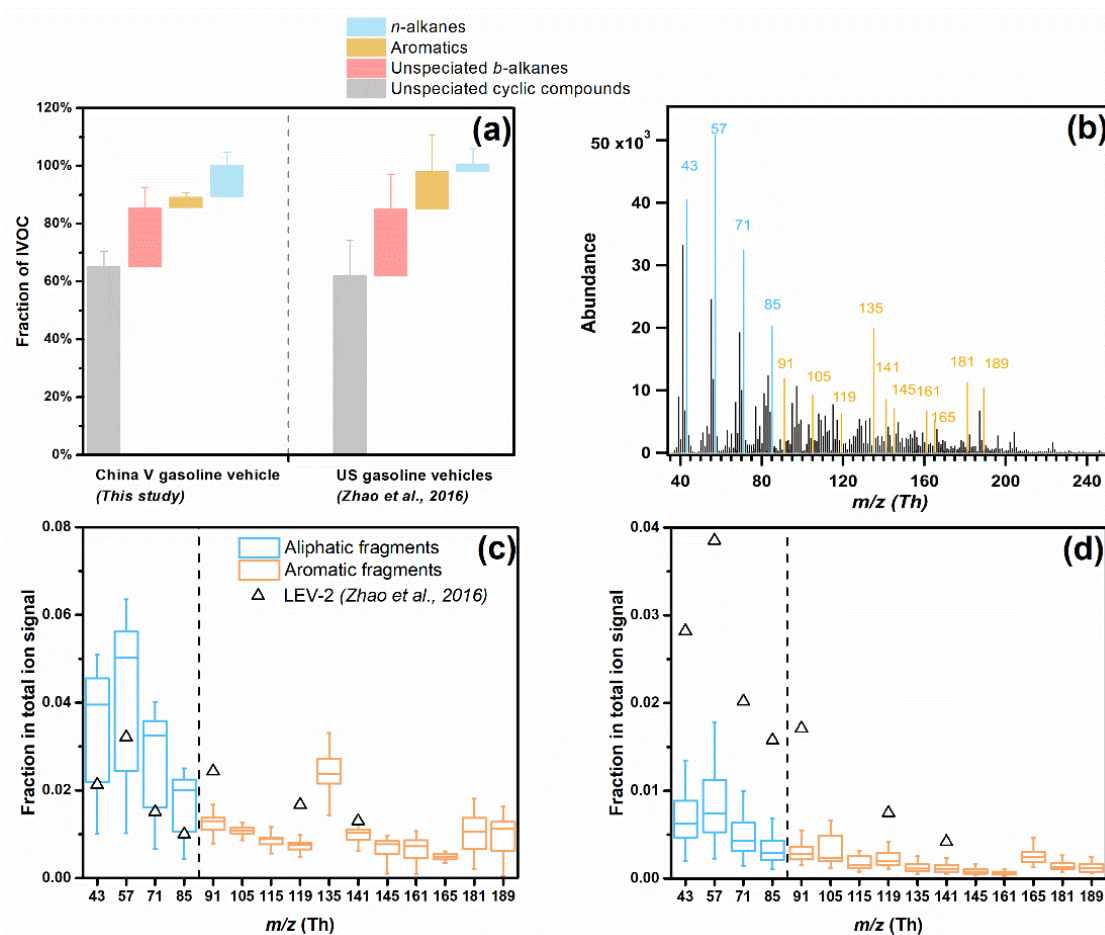
860 **Figure 5** Comparison of POA and estimated SOA production after 48 h of  
861 photo-oxidation (a) under low NO<sub>x</sub> condition; (b) at an OA loading of 10 μg·m<sup>-3</sup>  
862 under high NO<sub>x</sub> condition; (c) at an OA loading of 20 μg·m<sup>-3</sup> under high NO<sub>x</sub>  
863 condition; (d) at an OA loading of 80 μg·m<sup>-3</sup> under high NO<sub>x</sub> condition. The blue  
864 circles represent the SOA-to-POA ratio after 48 h of photooxidation (right axis).

865



866

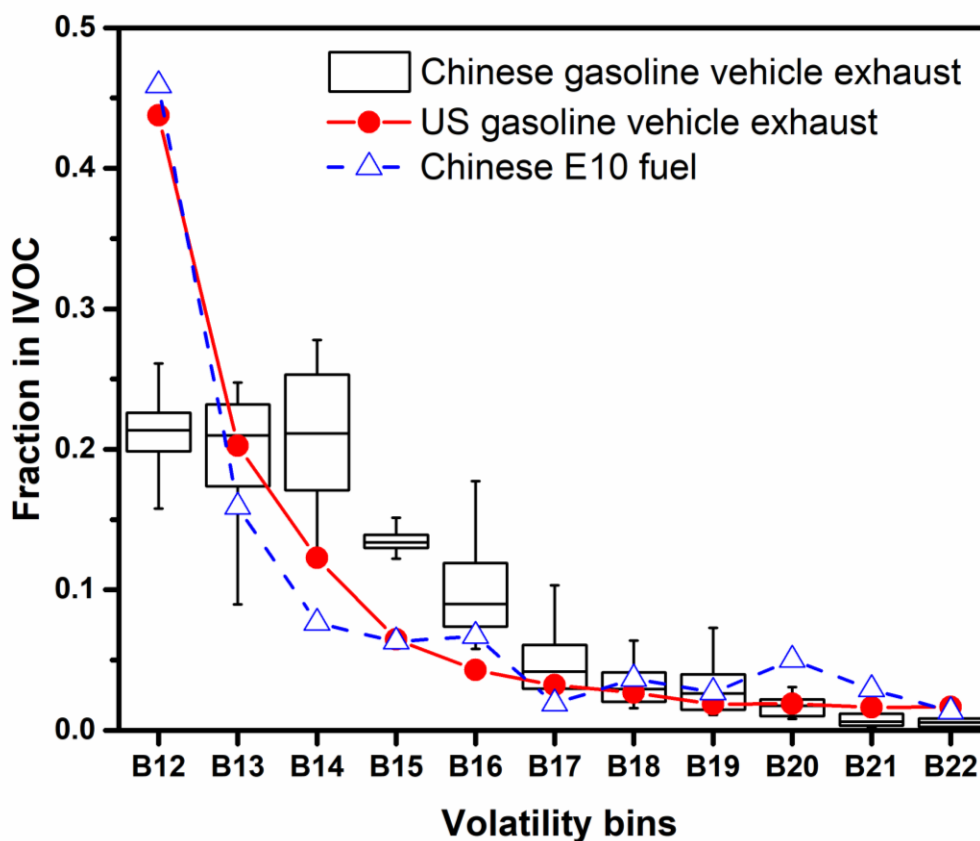
867 **Figure 1.** IVOC emission factors measured under different conditions, i.e. different  
 868 fuel type (gasoline, E10), test cycles (Chinese Light vehicles Test Cycle, CLTC, and  
 869 World-wide harmonized Light-duty Test Cycle, WLTC), starting mode (hot start and  
 870 cold start), and acceleration rates (acceleration rates of 1.2, 3.6 and 6.0 km/h/s). Stars  
 871 indicate the EF data from US, i.e. median US LEV-2 gasoline vehicles (vehicles  
 872 manufactured in 2004-2012), non-road construction machinery, and a large cargo  
 873 vessel (Qi et al., 2019;Huang et al., 2018;Zhao et al., 2016). The first category “China  
 874 V” is the compilation of all the EF results from all of the CLTC and WLTC tests. The  
 875 boxes indicate the median value, with error bars represent one standard deviation.



876

877 **Figure 2.** (a) Comparison of average chemical speciation of IVOC emissions from  
 878 China V vehicle and US vehicles (Zhao et al., 2016); (b) Average mass spectrum of  
 879 the IVOC during a typical E10-fueled cold start CLTC test. (c-d) Box-whisker plots of  
 880 the fractional contribution of selected fragments to total IVOCs signal for tested  
 881 China V vehicle: (c)  $B_{12}$ - $B_{16}$  bins; (d)  $B_{17}$ - $B_{22}$  bins. The boxes represent the 25<sup>th</sup> and  
 882 75<sup>th</sup> percentiles with the centerline being the median. The whiskers are the 10<sup>th</sup> and  
 883 90<sup>th</sup> percentiles. Black hollow triangles represent median LEV-2 data from Zhao et al.  
 884 (2016) LEV-2 represents vehicles manufactured from 2004 to 2012. Fragments  
 885 colored in blue represent aliphatic compounds, while those colored in orange are  
 886 associated with aromatic compounds.

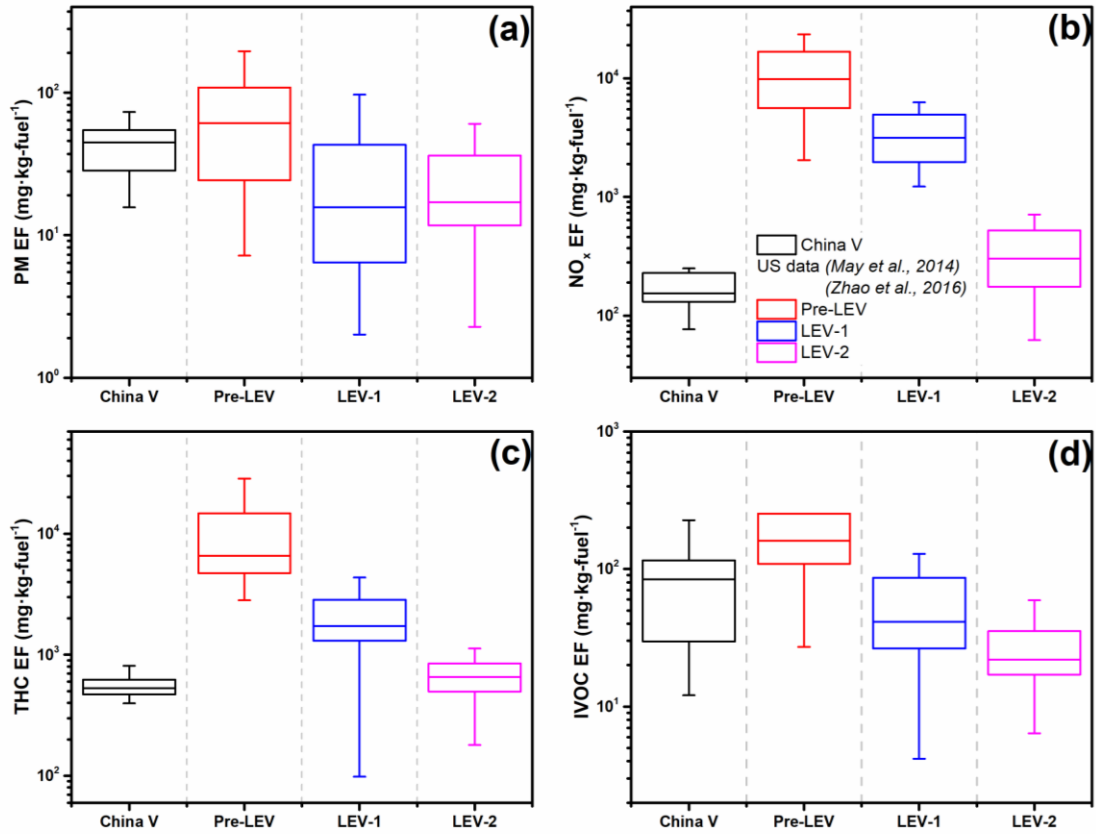
887



888

889 **Figure 3.** Comparison of IVOC volatility distributions of Chinese gasoline vehicle  
 890 exhaust, US gasoline vehicle exhaust, and Chinese E10 fuel (ethanol volume ratio of  
 891 10%, v/v). The box-plot represents the Chinese gasoline vehicle exhaust. The boxes  
 892 represent the 25<sup>th</sup> and 75<sup>th</sup> percentiles with the centerline being the median. The  
 893 whiskers are the 10<sup>th</sup> and 90<sup>th</sup> percentiles. Red solid circles represent IVOC fractions  
 894 of US vehicle exhaust (Zhao et al., 2016). Blue hollow triangles represent the IVOCs  
 895 volatility distribution of Chinese E10 fuel. As all the studies performed in US used  
 896 commercial US gasoline as fuel, which contained 10% v/v ethanol, i.e. E10 fuel.  
 897 Therefore, we compare the Chinese E10 with US fuel to get a consistent comparison.  
 898 Also, we should note that Zhao et al. (2016) and Lu et al. (2018) found that consistent  
 899 distribution of US fuel and exhaust, so in this figure, the US gasoline vehicle exhaust  
 900 can represent the volatility distribution of its unburned fuel distribution as well.

901

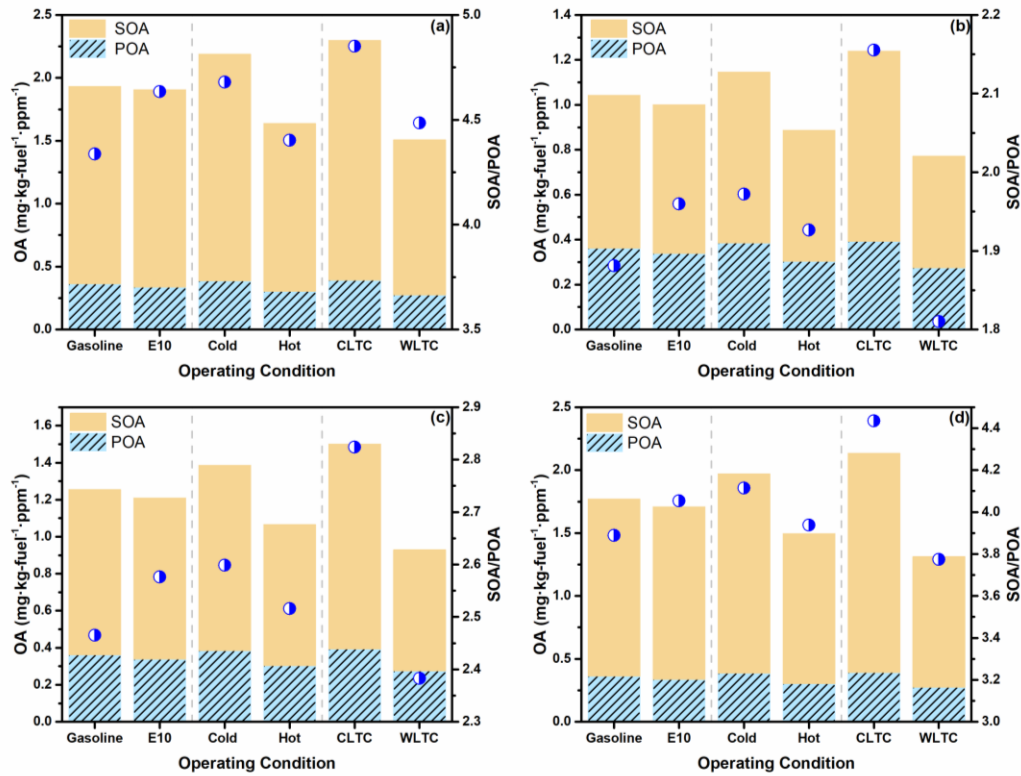


902

903 **Figure 4.** Comparison of emission factors of (a) PM (b)  $\text{NO}_x$  (c) THC, and (d) IVOC  
 904 between China and US on road gasoline vehicles (Zhao et al., 2016; May et al., 2014).

905 The boxes present the 75<sup>th</sup> and 25<sup>th</sup> percentiles with the centerline represents being the  
 906 median. The US vehicles are grouped by the model year, i.e. pre-LEV refers to  
 907 vehicles manufactured prior to 1994, LEV-1 represents vehicles from 1994-2003, and  
 908 LEV-2 is vehicles manufactured from 2004-2012.

909



910

911 **Figure 5** Comparison of POA and estimated SOA production after 48 h of  
 912 photo-oxidation (a) under low NO<sub>x</sub> condition; (b) at an OA loading of 10 μg·m<sup>-3</sup>  
 913 under high NO<sub>x</sub> condition; (c) at an OA loading of 20 μg·m<sup>-3</sup> under high NO<sub>x</sub>  
 914 condition; (d) at an OA loading of 80 μg·m<sup>-3</sup> under high NO<sub>x</sub> condition. The blue  
 915 circles represent the SOA-to-POA ratio after 48 h of photooxidation (right axis).

916

917

918